Available online at www.sciencedirect.com

ScienceDirect

journal homepage: www.elsevier.com/locate/he

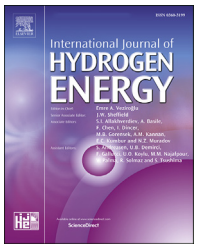

Comparative study of embrittlement of quenched and tempered steels in hydrogen environments

V. Arniella*, A. Zafra, G. Álvarez, J. Belzunce, C. Rodríguez

SIMUMECAMAT Research Group, University of Oviedo, Campus Universitario, 33203 Gijón, Spain

HIGHLIGHTS

- Hydrogen embrittlement is enhanced when the tests are performed with in-situ H-charging.
- Plastic straining at the notch tip severely increases hydrogen absorption.
- Martensite lath decohesion is the predominant failure mechanism in these tests.

ARTICLE INFO

Article history:
Received 24 November 2021
Received in revised form
23 February 2022
Accepted 19 March 2022
Available online 9 April 2022

Keywords:
Hydrogen embrittlement
42CrMo4 steel
Tensile test
Pre-charged specimens
In-situ hydrogen charging
Fracture micromechanisms

ABSTRACT

The study of steels which guarantee safety and reliability throughout their service life in hydrogen-rich environments has increased considerably in recent years. Their mechanical behavior in terms of hydrogen embrittlement is of utmost importance. This work aims to assess the effects of hydrogen on the tensile properties of quenched and tempered 42CrMo4 steels. Tensile tests were performed on smooth and notched specimens under different conditions: pre-charged in high pressure hydrogen gas, electrochemically pre-charged, and in-situ hydrogen charged in an acid aqueous medium. The influence of the charging methodology on the corresponding embrittlement indexes was assessed. The role of other test variables, such as the applied current density, the electrolyte composition, and the displacement rate was also studied. An important reduction of the strength was detected when notched specimens were subjected to in-situ charging. When the same tests were performed on smooth tensile specimens, the deformation results were reduced. This behavior is related to significant changes in the operative failure micromechanisms, from ductile (microvoids coalescence) in absence of hydrogen or under low hydrogen contents, to brittle (decohesion of martensite lath interfaces) under the most stringent conditions.

Introduction

In a global context of environmental awareness, one of the main objectives is to reduce the amount of CO_2 emitted into the atmosphere. The search for environmentally friendly and economical energy systems is the subject of much research. Hydrogen has recently emerged as an attractive energy source as it can be obtained from renewable sources such as wind, solar, hydro or geothermics. It is versatile and produces zero CO_2 emissions [1]. Therefore, the study of materials that can

* *Corresponding author.*
E-mail address: arniellavictor@uniovi.es (V. Arniella).
https://doi.org/10.1016/j.ijhydene.2022.03.203

safely and economically store and transport hydrogen under high pressure has become a topic of special interest [2].

The effects of hydrogen on metallic materials have been studied for many years [3]. Hydrogen embrittlement (HE) is a process in which hydrogen accumulates in specific microstructural regions, such as grain boundaries and other internal interfaces, reducing their cohesive strength and promoting sub-critical failure [4].

HE begins with the ingress of hydrogen in the alloy. This can take place during fabrication and processing (casting, chemical cleaning, pickling, electroplating, electrochemical machining, cathodic protection and welding). Hydrogen can also enter into the metal through an external source, such as cathodic electrochemical reactions at low temperatures (corrosion) or gaseous hydrogen exposure at high pressures or at elevated temperatures [5].

Once hydrogen has been absorbed into the metal, hydrogen atoms diffuse through its microstructure and some of them are trapped in "hydrogen traps". Hydrogen traps reduce hydrogen diffusivity and foster hydrogen accumulation in certain microstructural locations. These are determining factors for the initiation and propagation of cracks [6–8]. Although the effect of hydrogen on metallic materials has been extensively studied, the mechanism behind it is not yet fully understood. It is known that the absorption of hydrogen, its diffusion, and the microstructure of the steel are key factors in this process. Several mechanisms have been accepted to describe hydrogen-induced failures in metals. In steels the best known are hydrogen enhanced localized plasticity (HELP) [9–11], hydrogen enhanced decohesion (HEDE) [12,13], hydrogen adsorption induced by dislocation emission (AIDE) [14], and hydrogen-enhanced strain-induced vacancies (HESIV) [15].

Austenitic stainless steels and aluminum alloys are very resistant to hydrogen embrittlement, partly due to their low hydrogen diffusion coefficient [16,17]. Austenitic stainless steels are currently the most widely used steels in applications which are subjected to strong hydrogen pressure, however, due to their low yield strength and high cost, they are not a good choice in many hydrogen applications [18]. On the other hand, medium strength CrMo quenched and tempered martensitic steels are a good choice for pressure vessels, pipes, compressors, valves, registers, sensors, etc. when handling hydrogen at high pressures (up to 100 MPa) [19], but the long-term mechanical performance of these steels in hydrogen rich environments is not yet enough clear. This is an issue which must be studied in order to offer these steels as an alternative which guarantees their performance, as failure could have catastrophic consequences [20,21].

There are three ways to study the mechanical properties of steels in high-pressure hydrogen environments. Firstly, in-situ tests under high hydrogen pressure. This type of installation is very expensive and not always available. Secondly, specimens can be pre-charged with hydrogen (electrochemically or under high pressure) before testing (ex-situ tests). Finally, in-situ tests using electrochemical hydrogen charging. In the case of ferrous steel specimens, hydrogen diffusion coefficients are quite high [22], resulting in a rapid loss of pre-charged hydrogen. Therefore, mechanical tests with simultaneous hydrogen charging processes are preferred in this case.

Numerous authors have applied all these hydrogen-charging methods to determine the hydrogen-embrittlement susceptibility of different steels, studying the effect of several parameters such as steel composition, grain size [23–26], displacement rate [27], pre-charging methodology [28], tempering temperature [29], steel microstructure [30,31] and steel alloying (with Mo or V) [32,33].

However, only a few have compared the different charging methods. Asadipoor et al. [34] studied hydrogen embrittlement in X70 pipeline steel by means of tensile tests under vacuum in-situ H-plasma charging (IHPC), and ex-situ electrochemical H-charging (EEHC), demonstrating that EEHC is more effective than IHPC when evaluating hydrogen embrittlement. The influence of the charging method was also evaluated by Alvarez et al. [35] comparing a gaseous hydrogen and an electrochemical charging method. In this work the authors studied the influence of these pre-charging methods on the hydrogen embrittlement of three steels: an S355 structural carbon steel, a quenched and tempered alloyed steel (H8), and a weld metal of a real CrMoV welded joint (WM) using Small Punch tests. Higher hydrogen embrittlement indexes, related to the energy consumed per unit of area, were always observed after electrochemical pre-charging. The differences were attributed to significant losses of hydrogen during the cooling process necessary before extracting the samples after the gaseous pre-charging.

The aim of this work was primarily to develop a simple methodology to study the mechanical behavior of a quenched and tempered 42CrMo4 steel in in-situ H-charging conditions. Secondly it aimed to compare the influence of hydrogen charging methodologies on the embrittlement of smooth and notched specimens by means of tensile tests. Ex-situ (after gaseous and electrochemical pre-charging) and in-situ (electrochemical charging) tests were performed. Other aspects studied were the influence of the amount of hydrogen introduced in the samples and the displacement rate applied in the corresponding tests.

Materials and methods

Steel and heat treatment

The material used in this study was a commercial 42CrMo4 steel whose chemical composition is presented in Table 1. It is a medium carbon steel alloyed with Cr and Mo. Both its strength and toughness as well as its high fatigue resistance, make this steel an ideal candidate for use in high-pressure hydrogen environments [36].

Table 1 – Chemical composition of 42CrMo4 steel (% weight).

	C	Cr	Mo	Mn	Si	P	S
42CrMo4	0.42	0.98	0.22	0.62	0.18	0.008	0.002

A plate of 42CrMo4 steel (250 × 250 × 12 mm) was submitted to a heat treatment consisting of austenitizing at 845 °C for 40 min, followed by quenching in room temperature water and tempering at 700 °C for 2 h.

Hydrogen charging

One set of specimens was pre-charged in gaseous hydrogen at high pressure. Another set was electrochemically pre-charged. A third set of specimens was submitted to in-situ mechanical testing via electrochemical H-charging. Fig. 1 shows the two kinds of hydrogen precharging of the specimens before their testing in air conditions (ex-situ tests, Fig. 1(a)) and also the arrangement used to perform in-situ hydrogen tensile tests (Fig. 1b).

Precharging methods

The gaseous pre-charge was carried out in a high-pressure reactor, designed according to ASTM G146 [37]. Prior to hydrogen charging, an oxygen-free environment is ensured through inert gas purging. To ensure the saturation of the specimens, the following charging conditions were employed: 19.5 MPa at 450 °C for 21 h [36]. Then, the reactor was cooled for 1 h until it reached 85 °C, at which temperature the specimens were extracted. Some hydrogen loss is unavoidable during this stage [36]. The pre-charged specimens were then placed in liquid nitrogen (−196 °C) to limit further hydrogen losses. Cylindrical samples of 10 mm in diameter and 30 mm in length were introduced into the reactor together with the tensile specimens in order to determine the hydrogen concentration at the beginning of the mechanical tests as well as its evolution during the ex-situ tests.

Two different electrolytes were used for electrochemical pre-charging: 1) an acid electrolyte based on a 1 M H_2SO_4 solution and, 2) the same solution plus 0.25 g/l of As_2O_3. The addition of As_2O_3 to the electrolyte hinders the recombination of hydrogen atoms ($H + H \rightarrow H_2$), so a higher concentration of hydrogen on the metal surface is generated and a higher hydrogen content is attained in the sample [38]. In order to vary the quantity of hydrogen introduced into the steel, two current densities; i_c, of 0.5 and 1 mA/cm^2 were used for electrochemical pre-charging from the aforementioned acid solution. For the same reason, the same electrolyte without As_2O_3 was also used under a current density of 1 mA/cm^2. Different pre-charging times, ranging from 1 to 6 h, were used (at least 3 tests per condition were performed) to determine the saturation time corresponding to each charge. In this case cylinders of 5 mm in diameter and 30 mm in length were used to evaluate the evolution of the hydrogen concentration. The same electrolytes and current densities were also employed in the in-situ hydrogen charging tensile tests.

For both the gaseous and electrochemical pre-charge the specimen surfaces were polished to ensure better hydrogen ingress. In addition, all the specimens were washed with water and acetone before pre-charging and also before the start of the in-situ tests.

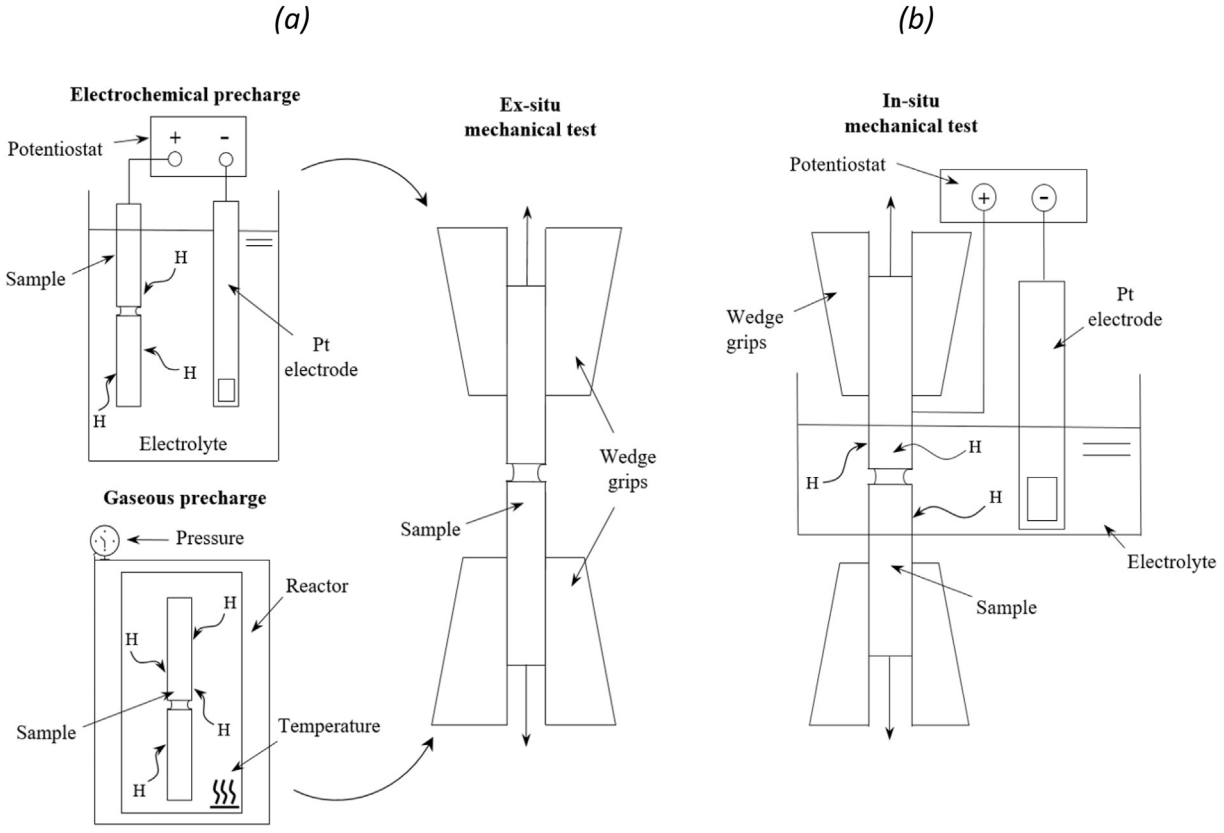

Fig. 1 – (a) Electrochemical and gaseous hydrogen pre-charging followed by ex-situ test (b) configuration to perform the in-situ hydrogen test.

Measurement of hydrogen content and diffusion simulation

The content of hydrogen introduced into the samples was measured by means of Thermal Desorption Analysis (TDA), using the cylindrical pins already described. For this purpose, a LECO DH603 hydrogen analyzer, able to measure hydrogen concentrations from 0.1 to 2500 ppm, was employed. The analysis measurement principle is based on the difference in thermal conductivity between a reference gas flow of pure nitrogen and a secondary flow composed on nitrogen and the hydrogen thermally extracted from the analyzed sample keeping the sample at 1100 °C for 400 s. The analyzer was previously calibrated using appropriate standards supplied by LECO.

The hydrogen flux, J, of the steel samples was also calculated by means of a simple uni-directional finite element analysis (FEA), implemented in an Abaqus commercial code, employing Fick's diffusion law, as described in Equation (1).

$$J = -D_{app}\nabla C_H \quad (1)$$

where D_{app} is the apparent hydrogen diffusion coefficient of the steel and C_H the hydrogen concentration. A certain hydrogen content on the sample surface, C_s, was imposed, being zero the hydrogen content in the rest of the sample. Finite element axisymmetric hydrogen diffusion analysis was performed on the radial direction using a cylindrical sample with a diameter of 5 mm, and assuming a room temperature hydrogen diffusion coefficient, D_{app} of 2.2 10^{-10} m^2/s [39]. The C_c/C_s ratio between the hydrogen content present in the center of the sample, C_c, and on its surface, C_s, was then calculated for different charging times.

Tensile tests

Tensile tests on both smooth and notched cylindrical specimens, whose geometries and dimensions are shown in Fig. 2, were performed at room temperature following the indications given by the ISO 6892-1 standard [40]. The circumferential notch had a depth of 2 mm and a notch tip radius of 0.15 mm, to give rise to a stress concentrator, k_t = 4.3 [36].

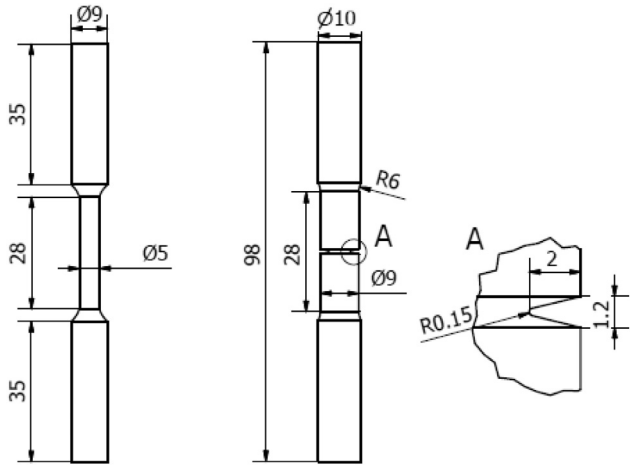

Fig. 2 – Smooth and notched tensile specimen geometry (in mm).

Longitudinal deformation of the specimens during the tests was measured by means of an extensometer with a calibrated length of 25 mm.

As a reference, as-received (AR) uncharged specimens of both geometries were first tested in laboratory conditions at a test displacement rate of 0.4 mm/min, according to tensile testing standards. In order to study the influence of this parameter on hydrogen embrittlement, displacement rates between 0.4 and 0.01 mm/min were used with hydrogen precharged specimens and also with in-situ tests. In the case of the notched specimens, tensile strength (σ_N) was defined as the maximum tensile load divided by the initial cross-sectional area of the notch region. The effect of hydrogen embrittlement was quantified through the hydrogen embrittlement index (HEI), which is defined by equation (2). HEI varies from 0%, (no embrittlement at all), to 100%, (maximum embrittlement).

$$HEI\ [\%] = \frac{X - X_H}{X} \cdot 100 \quad (2)$$

where, X and X_H are the measured steel properties evaluated without and with hydrogen, respectively.

Microstructure and fracture surfaces

The microstructure of the steel and the fracture surfaces of the tested specimens were observed in a scanning electron microscope (SEM JEOL-JSM5600) under a voltage of 20 kV. For the microstructural examination, the samples were ground, polished in synthetic cloths with diamond pastes of 6 and 1 μm, and finally chemically etched with Nital-2%. Vickers hardness measurements, HV30, were also performed applying a load of 30 kg for 15 s.

Results and discussion

Microstructure of the 42CrMo4 steel

Fig. 3 shows the tempered martensite microstructure of the steel under 5000× and 10000× magnifications. Carbide precipitation (iron/chromium carbides) is notorious during the tempering stage. As a high tempering temperature was applied (700 °C), internal stresses induced in the quench stage were relaxed and carbides precipitated and grew to attain a uniform distribution with a quasi-globular shape [36]. A Vickers hardness of 223 was also measured.

Hydrogen saturation curves

Hydrogen measurements at different charging times in a 1 M H_2SO_4 solution with 0.25 g/l of As_2O_3 with a density current of 0.5 mA/cm^2 and its fitting to the FEA model results are plotted in Fig. 4. The relation C_c/C_s between the hydrogen content present in the center of the sample, C_c, and on its surface, C_s, numerically calculated using Equation (1) is also shown (this curve does not depend on the hydrogen content on the sample surface). It is noted that approximately 90% of the surface hydrogen concentration is expected to be attained in the center of the sample after 3 h. In these conditions an average

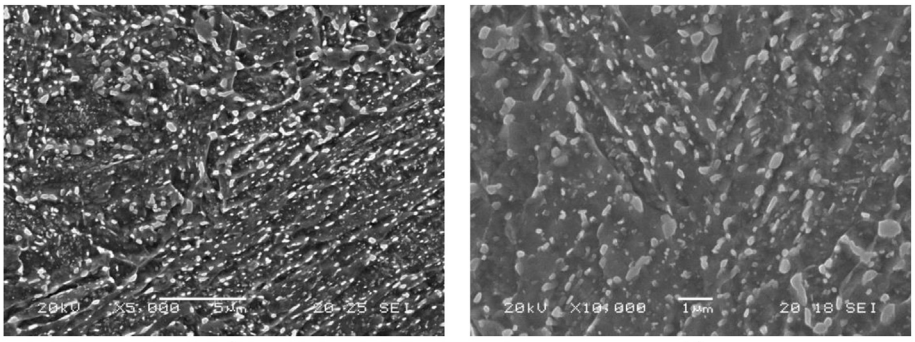

a) b)

Fig. 3 – a) SEM micrographs of the heat treated 42CrMo4 steel, and b) detail form the microstructure.

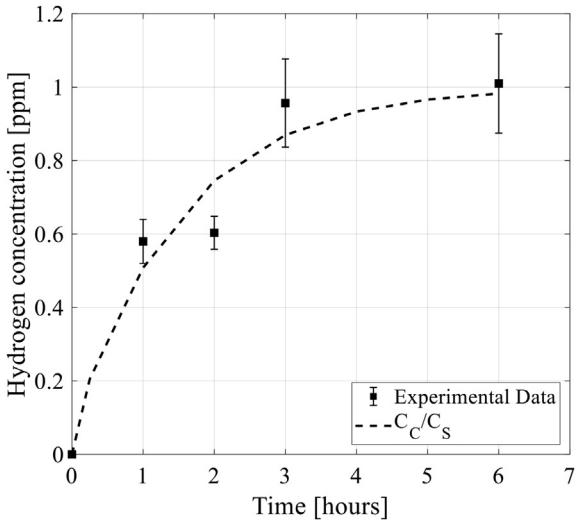

Fig. 4 – Experimental data and simulated hydrogen diffusion results, C_c/C_s (1 M H_2SO_4 solution with 0.25 g/l of As_2O_3, with a density current of 0.5 mA/cm^2).

hydrogen content of 0.95 ppm was measured after a charging time of 3 h, and of 1.01 ppm after 6 h. Based on these results, a pre-charging time of 3 h was chosen for all the ex-situ tests (near-saturation condition).

Various electrochemical charging conditions were tested for a fixed time of 3 h in order to introduce different amounts of hydrogen into the steel samples. The pre-charging tested conditions and the obtained results are presented in Table 2.

Table 2 – Hydrogen content after different pre-charging conditions (electrochemical pre-charging time was always 3 h).

Charging condition	C_H (ppm)
1 M H_2SO_4 solution, with As_2O_3 (1 mA/cm^2)	1.2
1 M H_2SO_4 solution, with As_2O_3 (0.5 mA/cm^2)	0.95
1 M H_2SO_4 solution (1 mA/cm^2)	0.5
Gaseous pre-charging	1.2

The influence of the applied current density and the strong effect of As_2O_3 addition, which avoids hydrogen atomic recombination, is observed. It is also worth noting that one of the applied electrochemical conditions was able to introduce the same amount of hydrogen as in the gaseous pre-charging (1.2 ppm).

Tensile tests and fracture analysis

Notched specimens

Hydrogen pre-charged specimens. Results obtained from ex-situ tensile tests performed with notched specimens on the reference (non-charged), gaseous, and electrochemical pre-charged samples are shown in Table 3.

Mean values of the notched tensile strength, σ_N, together with the corresponding embrittlement index, HEI, and the embrittled depth (measured on the failure surface) are recorded in Table 3. This table also shows the applied displacement rate and the time consumed in each test.

Hydrogen embrittlement indexes were very low (less than 6%) in all the gaseous pre-charged tests but increased slightly as the displacement rate decreased. However, for the slowest applied displacement rate (0.004 mm/min), HEI decreased again due to hydrogen loss in the course of the test, which had a total duration of 14 h.

When the notched specimens were electrochemically pre-charged, although similar initial hydrogen contents were measured on both set of tests, the HEIs were significantly higher than those obtained after gaseous pre-charging. In addition, a clear influence of the applied test rate is also observed, increasing from 7.5% to 13.8% when the displacement rate decreased from 0.4 to 0.1 mm/min.

Table 3 also shows the embrittled depth, which was measured in the scanning electron microscope on the failed surfaces. This is another sign of embrittlement that will be explained in the failure analysis section.

In-situ H-charged tests. The in-situ H-charged tests were carried out using two different electrolytes (1 M H_2SO_4 with and without As_2O_3 poison) and two different current densities (0.5 mA/cm^2 and 1 mA/cm^2). The results obtained are shown in Table 4.

Whatever the test condition used, the hydrogen embrittlement indexes measured with in-situ hydrogen charging

Table 3 – Notched tensile strength (σ_N) and embrittlement index (HEI) corresponding to notched tensile tests performed on pre-charged specimens.

Pre-charging method	C_H (ppm)	Displacement Rate (mm/min)	Time (min)	σ_N (MPa)	HEI (%)	Embrittled depth (mm)
AR	–	0.4	12	1330	–	–
Gaseous pre-charging	1.2	0.4	9	1273	4.3	0
		0.04	80	1258	5.4	0
		0.004	840	1294	2.7	0
Electrochemical pre-charging	1.2	0.4	10	1230	7.5	0.1
1 M H_2SO_4 + As_2O_3		0.1	44	1146	13.8	0.3
i = 1 mA/cm^2						

Table 4 – Notched tensile strength (σ_N) and embrittlement index (HEI) corresponding to notched tensile tests performed with in-situ hydrogen charging.

H-charging conditions	Dis.Rate (mm/min)	Time (min)	σ_N (MPa)	HEI (%)	Embrittled depth (mm)
AR	0.4	12	1330	–	–
1 M H_2SO_4 + As_2O_3	0.4	11	1069	19.6	0.51
i = 1 mA/cm^2	0.1	38	931	30.0	0.87
1 M H_2SO_4 + As_2O_3	1	6	1155	13.2	0.34
i = 0.5 mA/cm^2	0.4	15	1129	15.1	0.40
	0.1	51	1094	17.7	0.75
	0.05	112	972	26.9	0.80
	0.02	198	1030	22.6	0.78
	0.01	266	882	33.7	0.84
1 M H_2SO_4	1	7	1173	11.8	0.26
i = 1 mA/cm^2	0.4	16	1131	14.9	0.32
	0.1	59	1124	15.5	0.58
	0.05	158	1115	16.2	0.68
	0.02	225	1134	14.7	0.42
	0.01	456	1124	15.5	0.63

were much higher than those obtained with hydrogen pre-charged specimens. Moreover, embrittlement indexes increased with the hydrogen activity of the environment (higher current density and As_2O_3 addition) and with the decrease of the displacement rate. In this latter case, the displacement rate influence was small in tests performed with the low hydrogenated medium (H_2SO_4 without arsenic oxide).

Fracture analysis. The fracture surface of all the specimens was observed with the SEM in order to identify the operative fracture micromechanisms. The only failure mechanism present in the as-received steel (AR) was fully ductile, characterized by microvoid coalescence (MVC), as can be seen in Fig. 5(a). In the case of the specimens pre-charged in gaseous hydrogen, the same MVC micromechanism was also observed, and the action of hydrogen was only evidenced by the presence of shallow elongated dimples, shown in Fig. 5(b). These singular characteristics are generally associated with strain localization ahead of the notched region due to local accumulation of hydrogen, following the mechanism described as hydrogen-enhanced localized plasticity (HELP). The same mechanism was also observed in the electrochemically pre-charged specimens. However, as seen in Fig. 5(c), a thin flat region just ahead of the notch front was also observed in this latter case. This region was identified as a brittle zone in which the observed micromechanism was transgranular fracture. This took place following a hydrogen-enhanced decohesion (HEDE) mechanism, consisting of decohesion of the martensite lath interfaces (MLD, Fig. 5(d)) [36,41].

Fig. 6 shows typical examples of the fracture surfaces of the in-situ charged specimens. In all of them, two regions with differentiated failure mechanisms are present (Fig. 6(a)): ductile fracture in the center (Fig. 6(b), MCV), and transgranular fracture in the peripheral region extending from the front of the notch (Fig. 6(c), MLD). The detailed view of this region presented in Fig. 6(c) corresponds to the action of a decohesive embrittlement mechanism, with decohesion taking place along the interfaces between martensitic laths (MLD). Important secondary cracks mostly concentrated in the area between the aforementioned two regions were also visible in Fig. 6(a).

The failure of the specimens in the tests performed under in-situ hydrogen charging starts in the region located just ahead of the notch, where maximum of both normal and

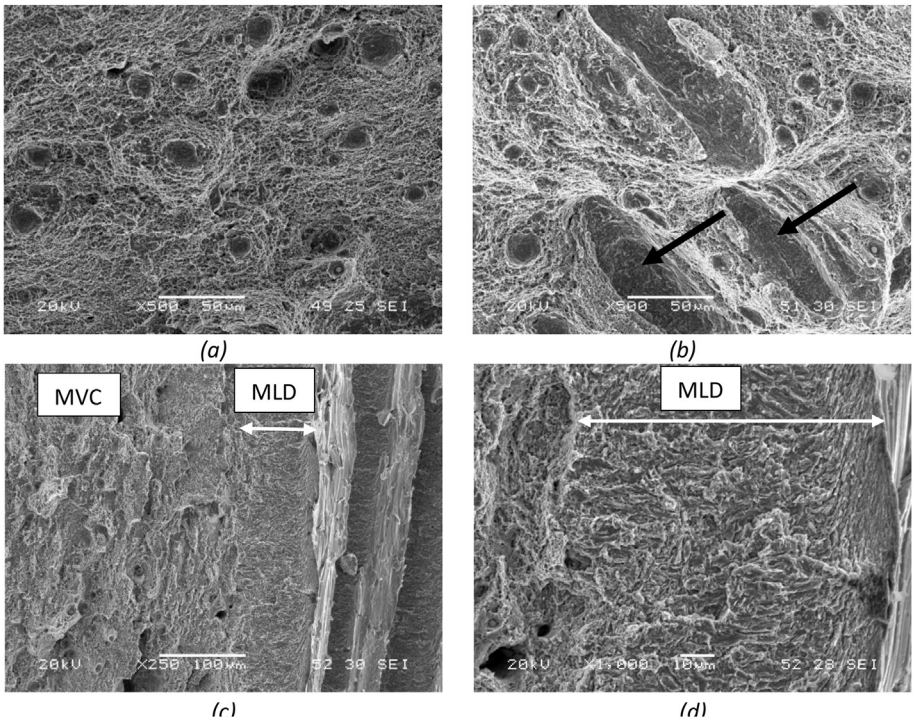

Fig. 5 – Fracture micromechanisms in notched tensile specimens: (a) reference uncharged sample, (b) gaseous pre-charged, (c, d) electrochemically pre-charged specimens.

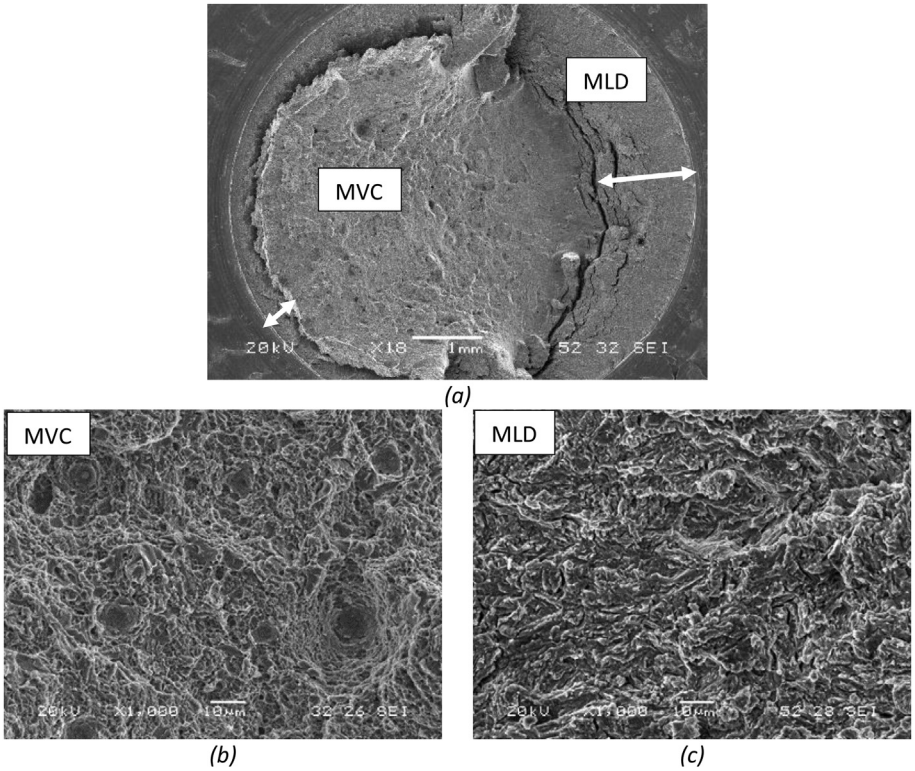

Fig. 6 – Fracture micromechanisms. In-situ H-charged notched tensile specimen at 0.5 mA/cm^2 and 0.05 mm/min, (a) general view, (b) MVC micromechanism, and (c) MLD micromechanism.

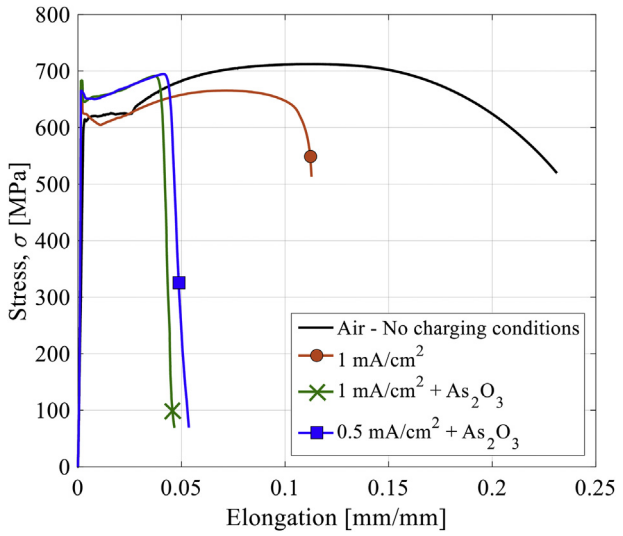

Fig. 7 – Smooth tensile tests under in-situ hydrogen charging. Stress-elongation curves.

hydrostatic stresses are generated. Hydrogen accumulates progressively in this region throughout the charging process triggering the aforementioned decohesion mechanism [42].

Smooth specimens

Based on the fact that hydrogen embrittlement was negligible when pre-charged notched specimens were used, it was decided to test the smooth tensile specimens under only in-situ H-charging at the lowest displacement rate, 0.01 mm/min. Fig. 7 and Table 5 show the results from these tests using different electrolytes and current densities.

Table 5 resumes the mean values of different tensile properties, yield stress, σ_{ys}; ultimate tensile strength, σ_{ut}; elongation at failure, e; and reduction of area, RA. This table also shows the hydrogen embrittlement indexes obtained using the three last parameters: $HEI_{\sigma ut}$, HEI_e, and HEI_{RA}. Yield and ultimate tensile strengths are barely affected by the ingress of hydrogen (embrittlement indexes below 5%). However, in the test performed with a current density of 1 mA/cm^2 and using As_2O_3 in the electrolyte significant embrittlement was observed both in elongation and in reduction of area, reaching embrittlement indexes of 91% and 87% respectively.

Failure always initiates in the center of the specimen transverse section, where the hydrostatic stress attains maximum values. As stated by other researchers [25,31,43] similar behavior was reported in in-situ tested smooth tensile specimens of different steels.

Fracture analysis. A fully ductile mechanism was observed in the referenced AR uncharged specimens, but failure micromechanisms observed in the in-situ H-charged smooth tensile specimens varied with the electrochemical charging conditions. The observed mechanism was fully brittle (MLD) when the electrolyte with As_2O_3 was employed, regardless of the applied current density: 1 mA/cm^2 (Fig. 8(a)) or 0.5 mA/cm^2 (8 (c)). On the contrary, only a ductile mechanism (MVC) was observed when the electrolyte without As_2O_3 (Fig. 8(b)) was used. The lower capacity to introduce hydrogen under this condition (0.5 ppm, Table 2) was unable to trigger the decohesion failure of the sample and microvoid coalescence was the only operative micromechanism.

Discussion

Hydrogen charging conditions

The importance of hydrogen charging conditions is clearly seen in Fig. 9(a), which compares the embrittlement indexes measured with gaseous and electrochemically pre-charged specimens with the results obtained by means of in-situ hydrogen charged tests performed on notched tensile specimens (1.2 ppm H were introduced under the three referred conditions, Table 2).

The same effect is seen in Fig. 9(b), related here to the depth of the peripheral embrittled region. The high HEI and embrittled depth found in the in-situ H-charging tests performed with low hydrogen activity, electrolyte without As_2O_3, i = 1 mA/cm^2 (16.2% and 0.68 mm, Table 4) are also noteworthy.

In order to explain these results, the elapsed time between the end of H-charging and the start of the mechanical test must be taken into account. When the gaseous pre-charging finishes, the samples must be cooled from 450 °C to 85 °C before they can be removed from the reactor. This process takes approximately 1 h. Significant hydrogen losses occur during this cooling stage. Hydrogen egress is especially significant in the region closest to

Table 5 – Tensile tests with in-situ hydrogen charging. Embrittlement indexes related to the yield strength, $HEI_{\sigma ys}$, ultimate tensile strength, $HEI_{\sigma ut}$, elongation, HEI_e, and reduction of area, HEI_{RA}.

H-charging conditions	Dis. Rate (mm/min)	Time (min)	σ_{ys} (MPa)	σ_{ut} (MPa)	$HEI_{\sigma ut}$ (%)	e (%)	HEI_e (%)	RA (%)	HEI_{RA} (%)
AR	0.4	20	622 ± 2	712 ± 5	–	23.4 ± 0.6	–	61.3 ± 1.7	–
1 M H_2SO_4 + As_2O_3 i = 1 mA/cm^2	0.01	321	646	691	3	2.1	91	8.0	87
1 M H_2SO_4 + As_2O_3 i = 0.5 mA/cm^2	0.01	305	657	697	2	3.0	87	9.7	84
1 M H_2SO_4 i = 0.5 mA/cm^2	0.01	459	636	683	4	14.5	38	37.8	38

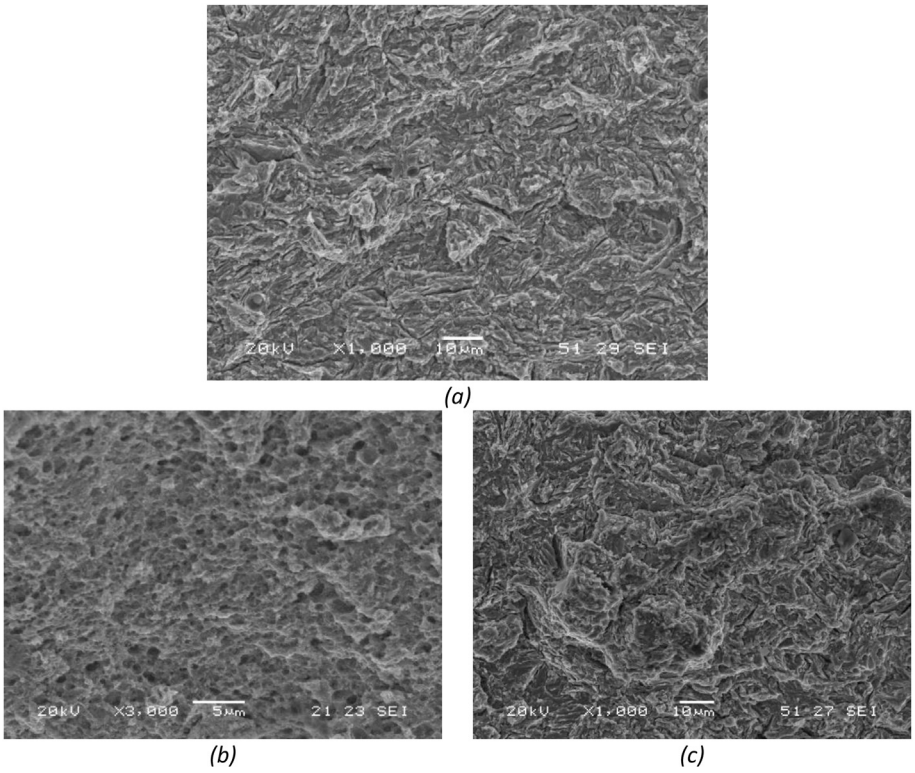

Fig. 8 – Fracture micromechanisms in in-situ H-charged smooth tensile specimens, (a) 1 mA/cm^2 with As_2O_3, (b) 1 mA/cm^2 without As_2O_3, (c) 0.5 mA/cm^2 with As_2O_3.

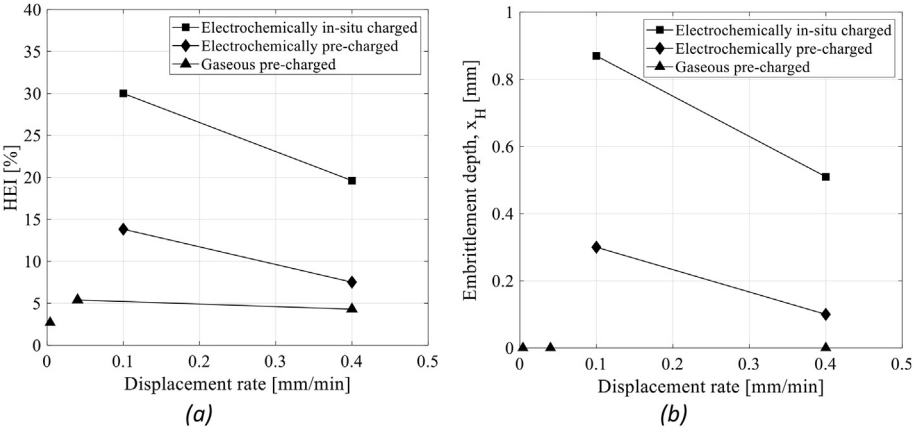

Fig. 9 – H pre-charged specimens and in-situ H tests, 1.2 ppm H, (a) hydrogen embrittlement indexes plotted against displacement rate, (b) measured embrittled depth against displacement rate.

the specimen surface, the region just ahead of the notch front where the fracture process initiates. However, in the electrochemical pre-charged specimens, when the mechanical test starts, hydrogen is uniformly distributed along the specimen section. Consequently, a higher hydrogen content is present in the process zone ahead of the notch than with gaseous pre-charging, leading to higher embrittlement indexes.

In the case of the in-situ H-charging tests, hydrogen is introduced while the specimen is mechanically loaded. Thus, hydrogen charging takes place when the steel is subjected to high levels of plastic deformation, especially in the region located just ahead the specimen notch. The effect of the degree of plastic deformation on this steel was studied by Zafra et al. [39,44]. In their research they performed build-up permeation transients on this same steel, subjected to different degrees of plastic pre-deformations. They used the same electrolyte with As_2O_3 employed in this work, starting with a density current of 0.5 mA/cm^2. The current was successively increased in 0.5 mA/cm^2 steps for the first two transients and then in 1 mA/cm^2 steps until saturation was reached. The measured subsurface hydrogen concentration at saturation was plotted in Fig. 10 against the applied plastic pre-deformation.

It can be seen that hydrogen concentration in equilibrium with the hydrogenated medium increases strongly with

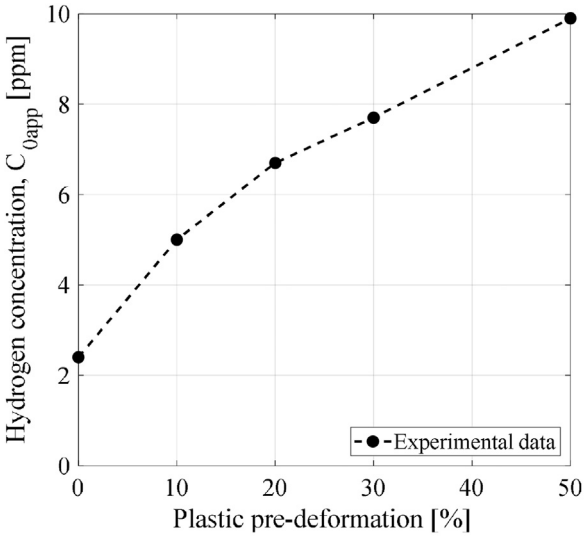

Fig. 10 – Hydrogen concentration at saturation against plastic pre-deformation. 42CrMo4 steel quenched and tempered at 700 °C (data from Ref. [44]).

applied plastic pre-deformation. More than a four-fold increase in hydrogen concentration was measured in this steel, from 2.4 ppm in the non-deformed sample to 9.9 ppm when a plastic pre-deformation of 50% was applied.

According to the Oriani theory [45], hydrogen atoms are attracted by the applied hydrostatic stress, σ_H, until an equilibrium hydrogen concentration, C_H, given by Equation (3) is attained:

$$C_H = C_0 e^{\frac{\sigma_H V_H}{RT}} \quad (3)$$

where C_0 is the diffusible hydrogen concentration in the absence of stress and V_H is the partial molar volume of hydrogen, approximately $2 \cdot 10^{-6}$ m^3/Hmol in a ferrous microstructure. Under these assumptions, the amount of hydrogen ahead of the notch region in the in-situ tests at failure was much higher than the C_0 concentration measured in non-deformed samples, and also significantly higher than the one existing in the process region in pre-charged specimens.

Fig. 11 shows the stress and strain distributions (hydrostatic stress, σ_H; and plastic strain, ε_p) in the notch region during an in-situ tensile test, and the entrance of hydrogen from a hydrogenated medium with hydrogen activity, a_H. The progressive evolution of the hydrogen distribution throughout the test (C_H^1, C_H^2, C_H^3…) until specimen failure is also shown in Fig. 11. Hydrogen accumulation in the process zone is driven by the hydrogen activity of the environment and particularly by the plastic strain in the front of the notch.

Notched strength threshold

Fig. 12(a) shows the evolution of the notched tensile strength with the applied displacement rate obtained in the in-situ tests performed with the electrolyte with As_2O_3 under 0.5 mA/cm^2 and with the same electrolyte without As_2O_3 under 1 mA/cm^2 (Table 4). The notched strength of the steel decreases with the displacement rate, as a longer time for hydrogen diffusion from the specimen surface to the process zone located ahead of the notch tip is available. Hydrogen atoms accumulate progressively in the martensite lath interfaces existing on the process zone of the specimen until the MLD brittle micromechanism is finally triggered and failure takes place.

The tensile strength of the notched specimens determined in the in-situ hydrogen charged tests performed under low hydrogen activity (electrolyte without As_2O_3) seems to saturate at displacement rates around 0.1 mm/min, to give a threshold strength of around 1100 MPa (corresponding to an HEI of 17%). However, under higher hydrogen activity (electrolyte with As_2O_3), the notched tensile strength of the steel decreases continuously with the displacement rate. The extrapolation of all these results to an extremely low displacement rate gives a threshold strength of approximately 850 MPa, which corresponds to an HEI of 36%.

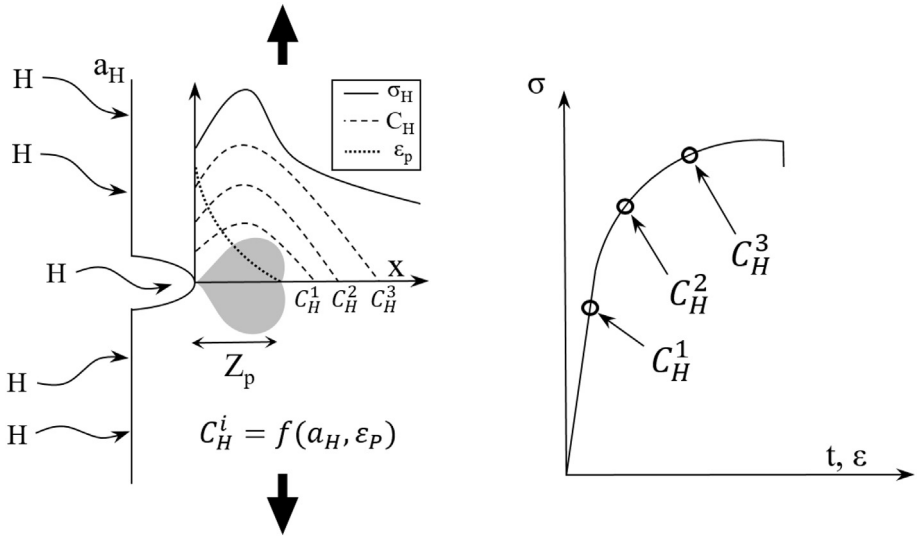

Fig. 11 – Scheme of the in-situ hydrogen-charged notch tensile test. Progressive hydrogen concentration distribution (C_H^1, C_H^2, C_H^3, …); hydrostatic stresses, σ_H; and plastic deformation, ε_p; at the notch tip. ZP is the plastic zone.

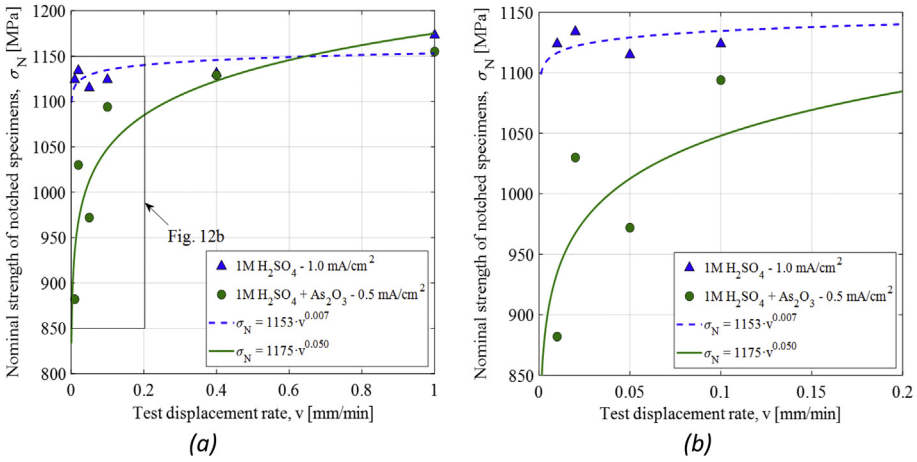

Fig. 12 – (a) Notched strength threshold determination in the in-situ hydrogen charged tensile tests (b) detail of (a).

Conclusions

Hydrogen embrittlement indexes measured with in-situ hydrogen charging of notched tensile specimens were much higher than those obtained with hydrogen pre-charged specimens. They increase with the hydrogen activity of the hydrogenated medium and with the decrease of the displacement rate applied in the test (longer time for hydrogen diffusion). In the case of the in-situ hydrogen charging tests, hydrogen is introduced while the specimen is mechanically loaded, so that hydrogen charging takes place while the steel surface is deforming plastically. Plastic deformation at the notch tip region can reach very high values, giving rise to a much greater accumulation of hydrogen in the process zone of the notched tensile specimens than in the hydrogen pre-charged ones.

Hydrogen accumulation in the process region of the notched tensile specimens induces a change in the failure micromechanism. When there is no hydrogen or when hydrogen concentration in the process region is low, the failure micromechanism is ductile (microvoid coalescence). Higher accumulations of hydrogen give rise to a brittle micromechanism, known as hydrogen-enhanced decohesion, HEDE, that involves decohesion of martensite lath interfaces in this particular quenched and tempered steel.

Embrittlement indexes related to strength are not relevant in the case of in-situ hydrogen charged tensile tests performed with smooth specimens, due to the absence of stress concentrators. However, they can attain very high values for elongation and reduction of area when high hydrogen concentrations are attained in specimens tested at very low displacement rates. Under these testing conditions, brittle martensite lath decohesion is also the predominant failure micromechanism.

Declaration of competing interest

The authors declare that they have no known competing financial interests or personal relationships that could have appeared to influence the work reported in this paper.

Acknowledgements

The authors would like to thank the Spanish Ministry of Science, Innovation and Universities for the financial support and FPI grant received to carry out research project RTI2018-096070-B-C31 (H2steel weld), and A. Zafra and G. Alvarez to the Ministry of Education and Culture of the Principality of Asturias for the Severo Ochoa grants PA-18-PF-BP17-038 and PA-20-PF-BP19-087.

REFERENCES

[1] Hydrogen roadmap Europe report. 2019. https://doi.org/10.2843/249013.
[2] Martin A, Agnoletti MF, Brangier E. Users in the design of hydrogen energy systems: a systematic review. Int J Hydrogen Energy 2020;45:11889–900. https://doi.org/10.1016/j.ijhydene.2020.02.163.
[3] Hirth JP. Effects of hydrogen on the properties of iron and steel. Metall Mater Trans 1980;11. https://doi.org/10.1007/BF02654700.
[4] Singh R, Singh V, Arora A, Mahajan DK. In-situ investigations of hydrogen influenced crack initiation and propagation under tensile and low cycle fatigue loadings in RPV steel. J Nucl Mater 2020;529:151912. https://doi.org/10.1016/j.jnucmat.2019.151912.
[5] Popov BN, Lee J, Djukic MB. Hydrogen permeation and hydrogen-induced cracking. 3rd ed. Elsevier Inc.; 2018. https://doi.org/10.1016/B978-0-323-52472-8.00007-1.
[6] Wang M. Determination of the critical hydrogen concentration for delayed fracture of high strength steel by constant load test and numerical calculation, vol. 48; 2006. p. 2189–202. https://doi.org/10.1016/j.corsci.2005.07.010.
[7] Ohaeri E, Eduok U, Szpunar J. Hydrogen related degradation in pipeline steel: a review. Int J Hydrogen Energy 2018;43:14584–617. https://doi.org/10.1016/j.ijhydene.2018.06.064.
[8] Haq AJ, Muzaka K, Dunne DP, Calka A, Pereloma EV. Effect of microstructure and composition on hydrogen permeation in X70 pipeline steels. Int J Hydrogen Energy 2013;38:2544–56. https://doi.org/10.1016/j.ijhydene.2012.11.127.

[9] Birnbaum H. Hydrogen-enhanced localized plasticity–a mechanism for hydrogen- related fracture. Mater Sci Eng 1994;176:191–202. https://doi.org/10.1016/0921-5093(94)90975-X.
[10] Birnbaum HK. Mechanisms of hydrogen related fracture of metals. 1989.
[11] Jagodzinski Y, Hänninen H, Tarasenko O, Smuk S. Interaction of hydrogen with dislocation pile-ups and hydrogen induced softening of pure iron. Scr. Mater. 2000;43:245–51. https://doi.org/10.1016/S1359-6462(00)00398-5.
[12] Pfeil LB. The effect of occluded hydrogen on the tensile strength of iron. In: Proceedings of the Royal Society of London. Series A, Containing Papers of a Mathematical and Physical Character; 1926. p. 182–95. https://doi.org/10.1098/rspa.1926.0103.
[13] Tarzimoghadam Z, Rohwerder M, Merzlikin SV, Bashir A, Yedra L, Eswara S. Acta Materialia Multi-scale and spatially resolved hydrogen mapping in a Ni e Nb model alloy reveals the role of the d phase in hydrogen embrittlement of alloy 718. Acta Mater 2016;109:69–81. https://doi.org/10.1016/j.actamat.2016.02.053.
[14] Lynch SP. Environmentally assisted cracking: overview of evidence for and adsorption-induced localised-slip process. Acta Metall 1988;36:2639–61. https://doi.org/10.1016/0001-6160(88)90113-7.
[15] Nagumo M. Hydrogen related failure of steels – a new aspect. https://doi.org/10.1179/026708304225019687; 2004.
[16] Turnbull A. Hydrogen diffusion and trapping in metals. Woodhead Publishing Limited; 2012. https://doi.org/10.1533/9780857095374.1.89.
[17] Stopher MA, Rivera-diaz-del-castillo PEJ. Hydrogen embrittlement in bearing steels. https://doi.org/10.1080/02670836.2016.1156810; 2016.
[18] Yamabe J, Awane T, Matsuoka S. Investigation of hydrogen transport behavior of various low-alloy steels with high-pressure hydrogen gas. Int J Hydrogen Energy 2015;40:11075–86. https://doi.org/10.1016/j.ijhydene.2015.07.006.
[19] Das T, Rajagopalan SK, Brahimi SV, Wang X, Yue S. A study on the susceptibility of high strength tempered martensite steels to hydrogen embrittlement (HE) based on incremental step load (ISL) testing methodology. Mater Sci Eng 2018;716:189–207. https://doi.org/10.1016/j.msea.2018.01.032.
[20] Murakami Y. The effect of hydrogen on fatigue properties of metals used for fuel cell system. Adv Fract Res 2007:167–95. https://doi.org/10.1007/978-1-4020-5423-5_10.
[21] Rajabipour A, Melchers RE. Service life of corrosion pitted pipes subject to fatigue loading and hydrogen embrittlement. Int J Hydrogen Energy 2018;43:8440–50. https://doi.org/10.1016/j.ijhydene.2018.03.063.
[22] Zhou X, Guo Y, Wang Z, Ma B, Ye X, Yang F, Rao Y, Jiang C, Chen C. Diffusion of hydrogen in China Reduced Activation Ferritic-martensitic steels at low temperatures. Fusion Eng Des 2019;143:59–65. https://doi.org/10.1016/j.fusengdes.2019.03.135.
[23] Martiniano GA, Silveira Leal JE, Rosa GS, Bose Filho WW, Piza Paes MT, Franco SD. Effect of specific microstructures on hydrogen embrittlement susceptibility of a modified AISI 4130 steel. Int J Hydrogen Energy 2021. https://doi.org/10.1016/j.ijhydene.2021.08.147.
[24] Noh HS, Kang JH, Kim SJ. Effect of grain size on hydrogen embrittlement in stable austenitic high-Mn TWIP and high-N stainless steels. Int J Hydrogen Energy 2019;44:25076–90. https://doi.org/10.1016/j.ijhydene.2019.07.227.
[25] Takasawa K, Ikeda R, Ishikawa N, Ishigaki R. Effects of grain size and dislocation density on the susceptibility to high-pressure hydrogen environment embrittlement of high-strength low-alloy steels. Int J Hydrogen Energy 2012;37:2669–75. https://doi.org/10.1016/j.ijhydene.2011.10.099.
[26] Thomas A, Szpunar JA. Hydrogen diffusion and trapping in X70 pipeline steel. Int J Hydrogen Energy 2019;45:2390–404. https://doi.org/10.1016/j.ijhydene.2019.11.096.
[27] de Almeida LFM, Oliveira SAG, Paes MTP, Ramos Neto FF, Franco SD, Arencibia RV. Effect of test velocity on the tensile strength of high strength steels using the small punch test in a hydrogen environment. Int J Pres Ves Pip 2021;194. https://doi.org/10.1016/j.ijpvp.2021.104552.
[28] Alnajjar M, Christien F, Bosch C, Wolski K. A comparative study of microstructure and hydrogen embrittlement of selective laser melted and wrought 17–4 PH stainless steel. Mater Sci Eng 2020;785. https://doi.org/10.1016/j.msea.2020.139363.
[29] Wang L, Cheng X, Peng H, Zhao PW, Cai ZX. Effect of tempering temperature on hydrogen embrittlement in V-containing low alloy high strength steel. Mater Lett 2021;302:130327. https://doi.org/10.1016/j.matlet.2021.130327.
[30] Michler T, Naumann J. Microstructural aspects upon hydrogen environment embrittlement of various bcc steels. Int J Hydrogen Energy 2010;35:821–32. https://doi.org/10.1016/j.ijhydene.2009.10.092.
[31] Ogawa Y, Hino M, Nakamura M, Matsunaga H. Pearlite-driven surface-cracking and associated loss of tensile ductility in plain-carbon steels under exposure to high-pressure gaseous hydrogen. Int J Hydrogen Energy 2021;46:6945–59. https://doi.org/10.1016/j.ijhydene.2020.11.137.
[32] Yi J, Zhuang X, He J, He M, Liu W, Wang S. Effect of Mo doping on the gaseous hydrogen embrittlement of a CoCrNi medium-entropy alloy. Corros Sci 2021;189:109628. https://doi.org/10.1016/j.corsci.2021.109628.
[33] Zhao H, Wang P, Li J. Effect of vanadium content on hydrogen embrittlement of 1400 MPa grade high strength bolt steels. Int J Hydrogen Energy 2021;46:34983–97. https://doi.org/10.1016/j.ijhydene.2021.08.060.
[34] Asadipoor M, Pourkamali Anaraki A, Kadkhodapour J, Sharifi SMH, Barnoush A. Macro- and microscale investigations of hydrogen embrittlement in X70 pipeline steel by in-situ and ex-situ hydrogen charging tensile tests and in-situ electrochemical micro-cantilever bending test. Mater Sci Eng 2020;772:138762. https://doi.org/10.1016/j.msea.2019.138762.
[35] Álvarez G, Zafra A, Belzunce FJ, Rodríguez C. Hydrogen embrittlement testing procedure for the analysis of structural steels with Small Punch Tests using notched specimens. Eng Fract Mech 2021;253:107906. https://doi.org/10.1016/j.engfracmech.2021.107906.
[36] Zafra A, Peral LB, Belzunce J, Rodríguez C. Effect of hydrogen on the tensile properties of 42CrMo4 steel quenched and tempered at different temperatures. Int J Hydrogen Energy 2018;43:9068–82. https://doi.org/10.1016/j.ijhydene.2018.03.158.
[37] ASTM. Standard practice for evaluation of disbonding of bimetallic stainless alloy/steel plate for use in high-pressure, high-temperature refinery. Cell 2001;1:1–6. https://doi.org/10.1520/G0146-01R13.1.
[38] Zakroczymski T. Adaptation of the electrochemical permeation technique for studying entry, transport and trapping of hydrogen in metals. In: Electrochim. Acta. Pergamon; 2006. p. 2261–6. https://doi.org/10.1016/j.electacta.2005.02.151.
[39] Zafra A, Belzunce J, Rodríguez C. Hydrogen diffusion and trapping in 42CrMo4 quenched and tempered steel: influence of quenching temperature and plastic deformation. Mater

Chem Phys 2020;255:123599. https://doi.org/10.1016/j.matchemphys.2020.123599.
[40] UNE-EN ISO 6892-1. Metallic materials. Tensile testing. Part 1: method of test at room temperature. 2019.
[41] Takeda Y, McMahon CJ. Strain controlled vs stress controlled hydrogen induced fracture in a quenched and tempered steel. Metall Trans A Phys Metall Mater Sci 1981;12 A:1255–66. https://doi.org/10.1007/BF02642339.
[42] Michler T, San Marchi C, Naumann J, Weber S, Martin M. Hydrogen environment embrittlement of stable austenitic steels. Int J Hydrogen Energy 2012;37:16231–46. https://doi.org/10.1016/j.ijhydene.2012.08.071.
[43] Park C, Kang N, Liu S. Effect of grain size on the resistance to hydrogen embrittlement of API 2W Grade 60 steels using in situ slow-strain-rate testing. Corros Sci 2017;128:33–41. https://doi.org/10.1016/j.corsci.2017.08.032.
[44] Zafra A. Study on hydrogen diffusivity and embrittlement of quenched and tempered 42CrMo4 steel. 2021.
[45] Oriani RA. The diffusion and trapping of hydrogen in steel. Acta Metall 1970;18:147–57.